Luminescence and a New Approach for Detecting Heat Treatment of Geuda Sapphire

Teerarat Pluthametwisute[1,2], Lutz Nasdala[2], Chutimun Chanmuang N.[2], Manfred Wildner[2], Eugen Libowitzky[2], Gerald Giester[2], E. Gamini Zoysa[3], Chanenkant Jakkawanvibul[4], Waratchanok Suwanmanee[4], Tasnara Sripoonjan[5], Thanyaporn Tengchaisri[6], Bhuwadol Wanthanachaisaeng[4] and Chakkaphan Sutthirat[1]

[1]Hub of Talents in Gem and Jewelry Industries, Department of Geology, Faculty of Science, Chulalongkorn University, 10330 Bangkok, Thailand;

[2]Institut für Mineralogie und Kristallographie, Universität Wien, 1090 Wien, Austria;

[3]Mincraft Co., 10370 Mount Lavinia, Sri Lanka;

[4]The Gem and Jewelry Institute of Thailand (Public Organization), 10500 Bangkok, Thailand;

[5]G–ID Laboratories, Bangkok, 10120, Thailand;

[6]Science and Technology Park (STeP), Chiang Mai University, 50200 Chiang Mai, Thailand.

Correspondence: Chakkaphan Sutthirat (email: chakkaphan.s@chula.ac.th)

Abstract. For decades, unravelling heat treatment of sapphire has been a challenging issue. The present study offers new aspects that support the detection of heat treatment of sapphire. Natural geuda sapphire exhibits orange to red luminescence under long–wave ultraviolet (LWUV, 365 nm) light, while heated geuda sapphire shows blue luminescence under short–wave ultraviolet (SWUV, 225 nm) light. The presence of melt inclusions in dissolved silks serves as an indicator of sapphire heat treatment. Fourier–transform infrared (FTIR) spectroscopy alone is insufficient for distinguishing unheated from heated sapphire. By combining orange to red luminescence with blue luminescence and melt inclusions, we provide a practical method for accurately differentiating natural gem–quality sapphire and heated gem–quality sapphire.

Keywords: gem; sapphire; heat treatment; luminescence

1 Introduction

Since the 1970s, Sri Lanka has been renowned for its gemstone resources, particularly geuda sapphire, a milky or silky corundum variety that is frequently heat–treated to enhance color and clarity (Ediriweera and Perera, 1989; Perera et al., 1991; Soysa and Fernando, 1992). High–temperature treatment of corundum (including ruby and sapphire) can significantly alter its milkiness, asterism, color, and internal features such as mineral inclusions (Nassau, 1981; Ediriweera and Perera, 1989; Hughes, 1997, 2017; Kyi et al., 1999;

38   Pisutha–Arnond, 2017; Themelis, 2018). Key factors in these transformations include the temperature,

39   duration, and atmospheric conditions of the heating process (Nassau, 1981; Emmett and Douthit, 1993;

40   Peiris, 1993; Emmett et al., 2003; Hughes, 2017; Pisutha–Arnond, 2017; Soonthorntantikul et al., 2019).

41   One of the first–rank challenges encountered by gemologists nowadays is the precise and

42   reliable identification of heat–treated ruby and sapphire. Blue luminescence under SWUV light, observed

43   in heated sapphire for over 50 years (Crowningshield 1966, 1970), can extend into the green region

44   (Nassau, 1981) and has been extensively studied (Evans, 1994; Wong et al., 1995a; Wong et al., 1995b;

45   Hughes 1997; McClure and Smith, 2000; Page et al., 2010; Alombert–Goget et al., 2016a; Alombert–Goget

46   et al., 2016b; Hughes, 2017; Vigier et al., 2021a, b, 2023). This luminescence may relate to rutile inclusions

47   commonly found in natural blue sapphire (Hughes, 2017). During heating at around 1600 °C, rutile

48   decomposes, incorporating Ti^{4+} ions into the sapphire structure (Sutthirat et al., 2006). Blue luminescence

49   serves as a key indicator of heat treatment in sapphire (Crowningshield, 1966; McClure and Smith, 2000;

50   Hughes, 2017; Hughes and Perkins, 2019). However, changes in original brown silk inclusions and orange

51   luminescence in natural unheated sapphire, relative to blue luminescence in heated sapphire, have not been

52   thoroughly explored. The present study provides a novel approach by observing the transformations in silk

53   inclusions and luminescence in sapphire before and after heating.

54

55   **2 Materials and methods**

56

57   Natural unheated geuda sapphire (A–type) samples (as described by Vertriest et al., 2019) were separated

58   based on the appearance of silk inclusions into three distinctive groups, i.e., high–density–silk (HS), low–

59   density–silk (LS), and silk–free (SF) specimens (Fig. 1). Using an Enraf–Nonius Kappa single–crystal X–ray

60   diffractometer with a charge–coupled device (CCD) area detector, these samples were oriented (based on

61   10 frames at a crystal detector distance of 35 mm), cut and polished into wafers with surfaces parallel to

62   the *c*–axis. For chemical analysis using an electron probe micro–analyser (EPMA) system, slabs were

63   coated with carbon for conductivity.

64   Heating experiments were conducted using a high–temperature electric furnace, Linn–

65   HT–1800–Vac. Heating was performed under ambient atmospheric conditions without any additional

66   oxygen buffer. Experimental conditions involved the maximum temperature of 1650 °C, which was

67   maintained for 10 hours, prior to natural cooling down in the furnace. A heating rate of 300 °C per hour

68   was set to reach the maximum temperature. To minimize surface contamination, the samples were placed

69   into a highly purified alumina (Al_2O_3) crucible.

70   The refractive index of samples was measured by a gemological refractometer (Krüss,

71   model ER605) with 1.81 refractive index liquid. Specific gravity was determined by a hydrostatic weighing

72   balance, by weighing samples in water (with a drop of dishwashing detergent added to reduce surface

73   tension) and in air.

74   Micro–inclusions in all samples were imaged using an Olympus BX–series microscope

75   equipped with Olympus DP27 digital camera. The camera was operated using the Olympus Stream micro–

76   imaging software. Raman spectra of inclusions were acquired using a confocal Raman spectrometer Horiba

77   Jobin Yvon LabRAM–HR Evolution. Using 473 nm laser excitation (15 mW at the sample) and a 50×/0.50

78   objective lens, a spectral range of 100–1350 cm^{-1} Raman shift was recorded. Wavenumber calibration was

79   done using the Rayleigh line, resulting in wavenumber accuracy of better than 0.5 cm^{-1}. A spectral

80   resolution of ca. 1.2 cm^{-1} resulted from 800 mm focal length and an 1800 grooves/mm optical grating in

81   the monochromator system. For more details see Zeug et al. (2018).

82   Chemical compositions of the samples were determined using a JEOL JXA 8100 EPMA.

83   Analytical conditions were set to 15 kV accelerating voltage and a probe current of about 2.5×10^{-8} A with

84   electron beam focussed to <1 μm. Natural mineral and synthetic oxide references were selected suitably

85   for calibration, including fayalite (Fe_2SiO_4) for Fe, wollastonite ($CaSiO_3$) for Ca, synthetic corundum

86   (Al_2O_3) for Al, synthetic periclase (MgO) for Mg, synthetic quartz (SiO_2) for Si, potassium titanyl

87   phosphate ($KTiOPO_4$) for K and Ti, synthetic manganosite (MnO) for Mn, synthetic eskolaite (Cr_2O_3) for

88   Cr, synthetic gadolinium gallium garnet ($Gd_3Ga_5O_{12}$) for Ga, and synthetic lead vanadium germanium

89   oxide for V. Counting times were 600 s peak and 300 s background for all elements. The K–α line was

90   analysed for all elements except for Ga where the L–α line was measured. Analytical crystals were selected

91   appropriately including thallium acid phthalate (TAP) crystal for Si and Al; pentaerythriol (PET) crystal

92   for Ti, Mg, K, and Ca; lithium fluoride (LIF) crystal for V, Cr, Ga, Fe, and Mn. The detection limit

93   (estimated from threefold background noise) is approximated at 0.005 wt% or 50 ppm. Three spots in each

94   sample were analyzed.

95   Polarized optical absorption (also referred to as UV–VIS–NIR) spectra of samples were

96   recorded on double–sided polished crystal slabs in the spectral range of 35000–3500 cm^{-1}, covering the

97   near ultraviolet (UV), the visible (VIS) and the near infrared (NIR) ranges. The measurements were

98   performed in the sample chamber of a Bruker Vertex 80 FTIR spectrometer at 2 mm measuring spot, using

99   a calcite Glan–prism polarizer and appropriate combinations of light sources (Xe or W lamp), beam splitters

100   (CaF_2–VIS/UV or CaF_2–NIR), and detectors (GaP, Si or InGaAs diodes) to cover the desired spectral

101   range. Hence, each full spectrum was combined from three partial spectra: 1) 35000–18000 cm^{-1} with 40

102   cm^{-1} spectral resolution and averaged from 256 scans; 2) 18000–9500 cm^{-1} with 20 cm^{-1} resolution and

103   256 scans; 3) 9500–3500 cm^{-1} with 10 cm^{-1} resolution and 128 scans.

104   Fourier–transform infrared spectra were acquired by means of a Bruker Tensor 27 FTIR

105   spectrometer attached to a Bruker Hyperion microscope in the spectral range from 4000 cm^{-1} to 1600 cm^{-1}.

106   A glowbar light source, a KBr beamsplitter, and a deuterated L–alanine doped triglycene sulphate

107   (dLATGS; Tensor27) or Hg–Cd–telluride (MCT) detector (Hyperion) were employed. The spectral

108   resolution was 4 cm^{-1}, sample and reference spectra were averaged from 128 scans.

109   Luminescence phenomena were observed and photo–captured both before and after heat

110   treatment. The images were obtained under LWUVillumination using ZEISS microscope model stemi 508

111   with 0.63× magnification. The images were captured in a darkened room using CANON digital single lens

112   reflex (DSLR) camera model EOS 80D (24.2 MP resolution), which was mounted on top of the microscope.

113   The Superfire UV (365 nm) mini flashlight model S11–H, 3W (max), DC 3.7 V, was held approx. 15 cm

114   above the samples. The camera settings involved an exposure time of 5 s, an exposure bias of 0 steps, and

115   an ISO speed of 200. The aperture was adjusted to f/0, and the focal length of 0 nm. For SWUV illumination

116 (approximately 225 nm), a DiamondView™ device was used. The parameter settings for DiamondView™

117 were established as follows: Integration duration: 2.83 s; minimum excitation status: Off. Power settings

118 ranged from 50% to 80%, contingent upon the intensity of luminescence. A gain of 13.85 dB is measured.

119 The aperture was set to 80% and the field stop to 67%. Gamma was disabled. Photoluminescence (PL)

120 spectra in the visible and near–infrared ranges were acquired using a confocal Horiba Jobin Yvon

121 LabRAM–HR 800 spectrometer. Spectra were excited using the 325 nm emission of a He–Cd laser (ca. 10

122 mW at the sample surface). The system was calibrated using emission lines of a Kr lamp. The spectral

123 resolution was in the range 0.07 nm (violet) to 0.02 nm (NIR range). All the spectra were acquired at the

124 same position both before and after heating experiments.
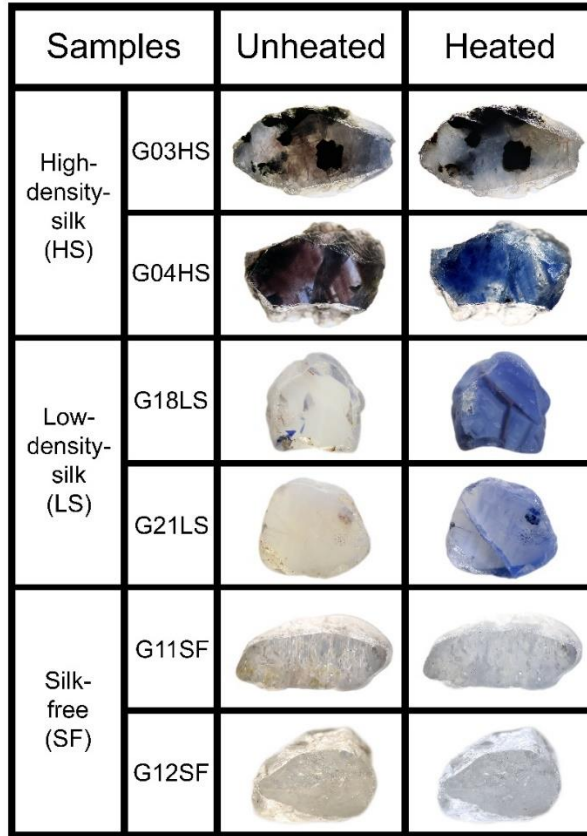
125

126 **3 Results**

127

128 **3.1 Heating–induced property changes and alteration**

129 Representatives of natural unheated and their heated counterparts of all groups are shown in Fig. 1. All the

130 samples ranged from a specific gravity of 3.83 to 4.08, and refractive indices of 1.760 to 1.770 falling well

131 within the range of corundum properties. Before heating, samples showed varying natural appearances

132 based on inclusion density. Geuda samples with HS inclusions (e.g., G03HS and G04HS, Fig. 1) exhibited

133 brown silk and brown color banding or zoning, while a few samples also displayed a natural blue color.

134 Samples with LS inclusions (e.g., G18LS and G21LS, Fig. 1) generally appeared milky with yellowish or

135 brownish tints. After heating, most samples turned blue, ranging from pale to dark shades, with the milky

136 appearance and yellowish or brownish tints significantly reduced. On the other hand, the SF group usually

137 showed a slightly yellowish appearance (Fig. 1, samples G11SF and G12SF). After the heating experiment,

138 they had changed slightly to a very pale blue color.

139

Samples		Unheated	Heated
High-density-silk (HS)	G03HS		
	G04HS		
Low-density-silk (LS)	G18LS		
	G21LS		
Silk-free (SF)	G11SF		
	G12SF		

Figure 1. Representatives of natural unheated geuda sapphire samples within three separate groups, i. e., HS (G03HS, G04HS), LS (G18LS, G21LS), and SF (G11SF, G12SF) groups, and their appearances after heating. Sizes of stones range between 4 and 12 mm.

3.2 Mineral chemistry

Chemical compositions of samples in the three distinct groups are summarized in Tables 1 to 3. The Al_2O_3 contents range between 98.2 and 99.5 wt%. Other elements are found as trace contents only, particularly Fe, Ti, and Ga. Fe and Ti are essential coloring elements in sapphire. The HS group contained the highest Fe contents of 0.32–0.36 wt% FeO, together with 0.02–0.04 wt% TiO_2 and <0.7 wt% Ga_2O_3. The LS group had a high Ti content of 0.02–0.51 wt% TiO_2 with $\leq$0.06 wt% FeO and $\leq$0.8 wt% Ga_2O_3. The SF group contained 0.06–0.26 wt% FeO, $\leq$0.04 wt% TiO_2 and <1 wt% Ga_2O_3.

153 **Table 1.** Representative chemical compositions (EPMA results) and calculated mineral formulae of HS

154 sapphire samples.

Samples	G01HS	G02HS	G03HS	G04HS
Major oxides (wt%):				
SiO_2	0.00	0.00	0.45	0.40
TiO_2	0.02	0.02	0.04	0.03
Al_2O_3	99.0	98.7	98.9	98.7
V_2O_3	0.01	0.00	0.00	0.03
Cr_2O_3	0.00	0.02	0.03	0.00
Ga_2O_3	0.62	0.66	0.00	0.39
FeO_{total}*	0.32	0.33	0.36	0.36
MnO	0.02	0.00	0.00	0.02
MgO	0.00	0.00	0.01	0.01
K_2O	0.00	0.00	0.00	0.00
CaO	0.01	0.01	0.02	0.01
Total	100.0	99.8	99.8	100.0
Mineral formulae (apfu)**:				
Si	0.000	0.000	0.008	0.007
Ti	0.000	0.000	0.001	0.000
Al	1.990	1.989	1.985	1.982
V	0.000	0.000	0.000	0.000
Cr	0.000	0.001	0.000	0.000
Ga	0.007	0.007	0.000	0.004
Fe	0.013	0.014	0.005	0.005
Mn	0.000	0.000	0.000	0.000
Mg	0.000	0.000	0.000	0.000
K	0.000	0.000	0.000	0.000
Ca	0.000	0.000	0.000	0.000
Sum	2.010	2.011	1.999	2.000

155 * FeO_{total} = total Fe oxide, assuming all Fe to be ferrous

156 ** Calculated based on 3 O atoms per formula unit

157

158 **Table 2.** Representative chemical compositions (EPMA results) and calculated mineral formulae of LS

159 sapphire samples.

| Samples	**G06LS**	**G16LS**	**G18LS**	**G20LS**	**G21LS**
Major oxides (wt%):					
SiO_2	0.00	0.00	0.11	0.00	0.00
TiO_2	0.04	0.27	0.37	0.51	0.02
Al_2O_3	99.0	98.5	98.4	98.3	98.6
V_2O_3	0.02	0.03	0.01	0.02	0.01
Cr_2O_3	0.00	0.06	0.00	0.02	0.00
Ga_2O_3	0.10	0.37	0.58	0.81	0.59
FeO_{total}*	0.00	0.06	0.06	0.06	0.05
MnO	0.01	0.00	0.00	0.00	0.01
MgO	0.02	0.02	0.01	0.01	0.02
K_2O	0.00	0.00	0.00	0.00	0.00
CaO	0.00	0.00	0.01	0.01	0.00
Total	99.2	99.3	99.6	99.7	99.3
Mineral formulae (apfu)**:					
Si	0.000	0.000	0.002	0.000	0.000
Ti	0.001	0.003	0.005	0.007	0.000
Al	1.997	1.989	1.984	1.981	1.992
V	0.000	0.000	0.000	0.000	0.000
Cr	0.000	0.002	0.000	0.001	0.000
Ga	0.001	0.004	0.006	0.009	0.007
Fe	0.000	0.002	0.002	0.002	0.002
Mn	0.000	0.000	0.000	0.000	0.000
Mg	0.001	0.001	0.001	0.000	0.001
K	0.000	0.000	0.000	0.000	0.000
Ca	0.000	0.000	0.000	0.000	0.000
Sum	2.001	2.003	2.000	2.000	2.002

160 * FeO_{total} = total Fe oxide, assuming all Fe to be ferrous

161 ** Calculated based on 3 O atoms per formula unit

162

163 **Table 3.** Representative chemical compositions (EPMA results) and calculated mineral formulae of SF
164 sapphire samples.

Samples	G07SF	G11SF	G12SF	G14SF	G22SF	G23SF
Major oxides (wt%):						
SiO_2	0.01	0.13	0.06	0.00	0.00	0.00
TiO_2	0.03	0.04	0.03	0.00	0.04	0.01
Al_2O_3	98.7	98.7	98.8	99.5	98.2	98.7
V_2O_3	0.00	0.02	0.00	0.00	0.00	0.00
Cr_2O_3	0.00	0.00	0.01	0.00	0.00	0.00
Ga_2O_3	0.71	0.00	0.00	0.15	0.78	0.94
FeO_{total}*	0.06	0.26	0.08	0.10	0.22	0.13
MnO	0.01	0.02	0.00	0.01	0.02	0.00
MgO	0.00	0.02	0.00	0.00	0.00	0.00
K_2O	0.00	0.01	0.00	0.00	0.00	0.00
CaO	0.02	0.00	0.02	0.01	0.01	0.01
Total	99.6	99.2	99.0	99.8	99.3	99.8
Mineral formulae (apfu)**:						
Si	0.000	0.002	0.001	0.000	0.000	0.000
Ti	0.000	0.001	0.000	0.000	0.001	0.000
Al	1.991	1.993	1.997	1.997	1.988	1.988
V	0.000	0.000	0.000	0.000	0.000	0.000
Cr	0.000	0.000	0.001	0.000	0.000	0.000
Ga	0.008	0.000	0.000	0.002	0.009	0.010
Fe	0.002	0.011	0.003	0.004	0.009	0.005
Mn	0.000	0.000	0.000	0.000	0.000	0.000
Mg	0.000	0.001	0.000	0.000	0.000	0.000
K	0.000	0.000	0.000	0.000	0.000	0.000
Ca	0.000	0.000	0.000	0.000	0.000	0.000
Sum	2.002	2.009	2.003	2.003	2.007	2.004

165 * FeO_{total} = total Fe oxide, assuming all Fe to be ferrous

166 ** Calculated based on 3 O atoms per formula unit

167

3.3 Microscopic features

Negative crystals, with or without CO_2 gas bubbles, were commonly observed alongside mineral inclusions, such as oligoclase feldspar, calcite, and muscovite, in these sapphire samples. Brown silk inclusions were prominent in both HS and LS groups, as shown in Fig. 2 (G22SF, G18LS, and G04HS for Fig. 2a, Fig. 2b–c, and Fig. 2d–f, respectively). Micro–Raman spectroscopy was used to identify CO_2 and mineral inclusions. Although brown silk inclusions, typically needle–shaped and aligned with color banding (Fig. 3a), were often less than 1 µm in diameter and difficult to identify, irregular or flaky platelet forms (Fig. 3c) were also noted.
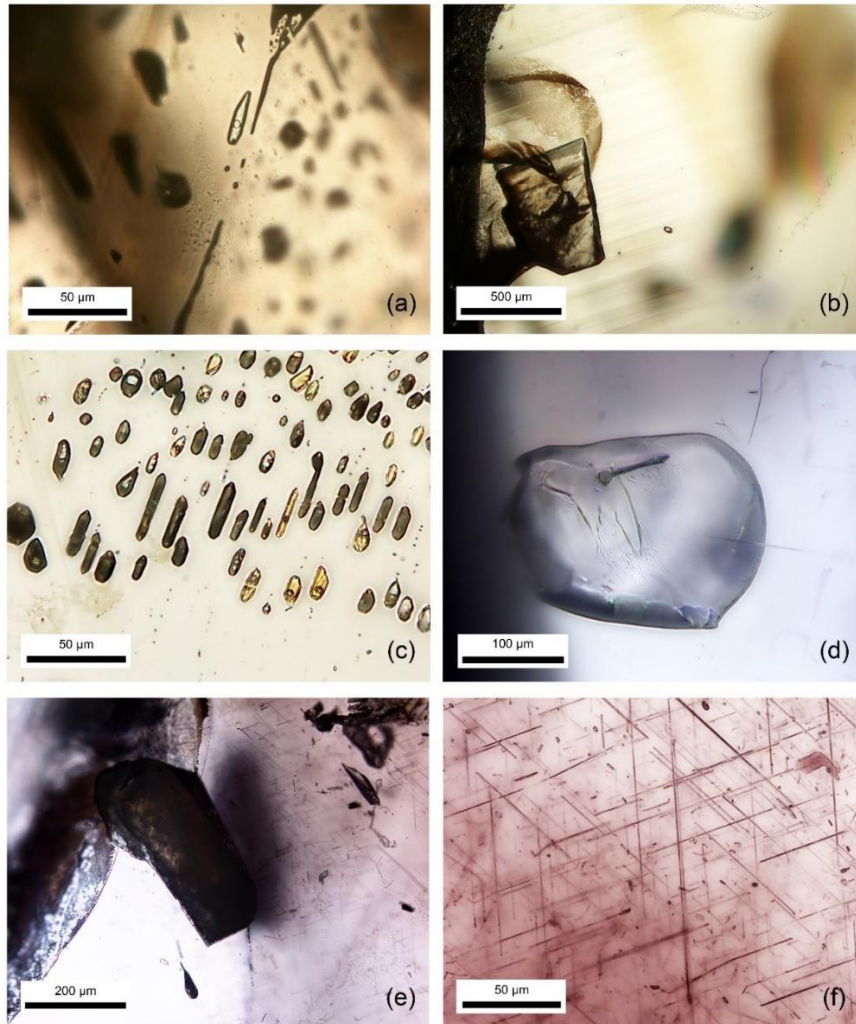
Figure 2. Transmitted–light photomicrographs of inclusions including CO_2–containing negative crystals **(a)**, calcite **(b)**, cluster of negative crystals **(c)**, oligoclase **(d)**, muscovite **(e)**, and brown silks **(f)** in natural unheated sapphire.

After high–temperature heating, molten surfaces (Fig. 3e) and decomposed crystal inclusions were commonly observed in these samples. The most notable alteration was also detected in the initial area of brown silks (Fig. 3a), which exhibited distinct bluish color banding/zoning (Fig. 3b) after heating.

185

186
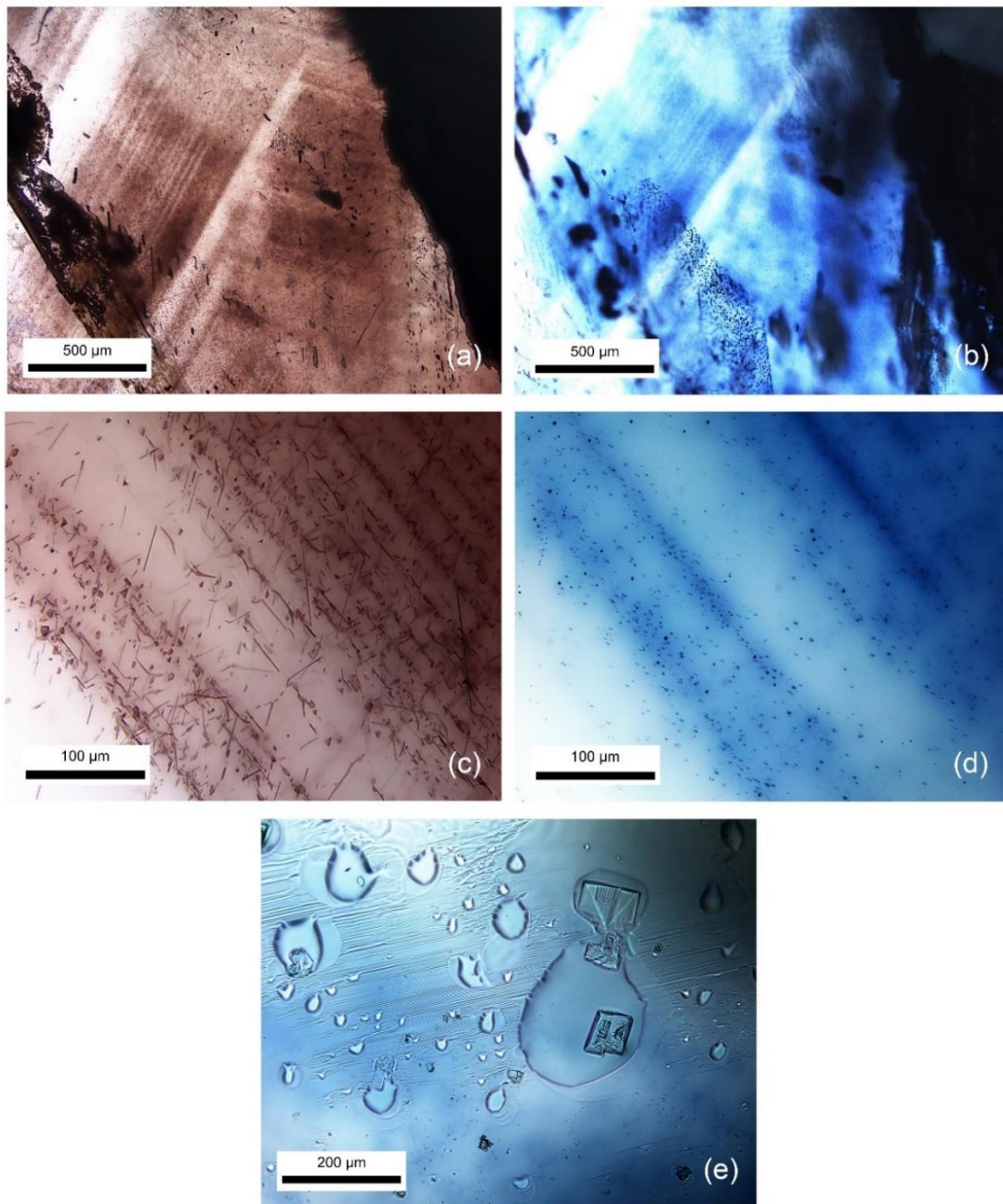
Figure 3. Transmitted–light photomicrographs showing that brown banding **(a)** with irregular platy brownish flakes and tiny needles **(c)** in natural unheated sapphire samplesample G04HS turned into blue color banding **(b)** with blue dots **(d)** upon heating. Melted surface **(e)** was also observed after heat treatment.

The brown silks (Fig. 3c) experienced a transformation upon heating into blue dots (Fig. 3d). Additionally, melt inclusions among blue dots were likely developed by melting of brown silks of the sapphire host, which have never been reported elsewhere, becoming significantly noticeable and useful for indicating heat treatment of sapphire (Fig. 4).

195
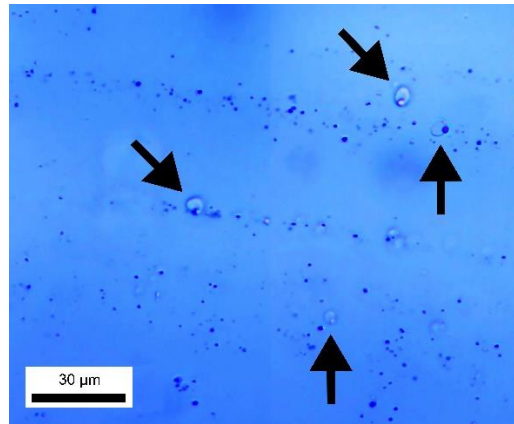
Figure 4. Transmitted–light photomicrograph showing melt inclusions (arrows) among blue dots transformed from silk inclusions in sapphire after heating (sample G04HS).

3.4 Optical (UV‑VIS‑NIR) spectroscopy

The optical spectra of representative sapphire samples are presented in Fig. 5. Absorption peaks at 374, 388, and 450 nm, as well as (broad) bands around 580 and 880 nm, were observed. Optical spectra have been studied on unheated and heated sapphire by numerous previous researchers (e. g., Ediriweera and Perera, 1989; Perera et al., 1991; Emmett and Douthit, 1993; Hughes, 1997; Kyi et al., 1999; Emmett et al., 2003; Sripoonjan et al., 2014; Hughes, 2017; Pisutha–Arnond, 2017; Themelis, 2018; Palke et al., 2019; Soonthorntantikul et al., 2019; Dubinsky et al., 2020). The 374, 388, and 450 nm peaks as well as the 880 nm band were proposed to be attributed to Fe, the 580 nm band to the Fe–Ti pair. After heating, all samples showed a significant increase in the main Fe–Ti pair related absorption band at around 580 nm (Figs. 5a–c), whereas Fe–Fe related absorption at around 880 nm was only increased in some samples (i.e., Figs. 5a and 5c). The intensified absorption of the 580 nm band in these samples is referred to an increase of Fe–Ti pairs after heating which leads to enhanced blue coloration in heated sapphires.
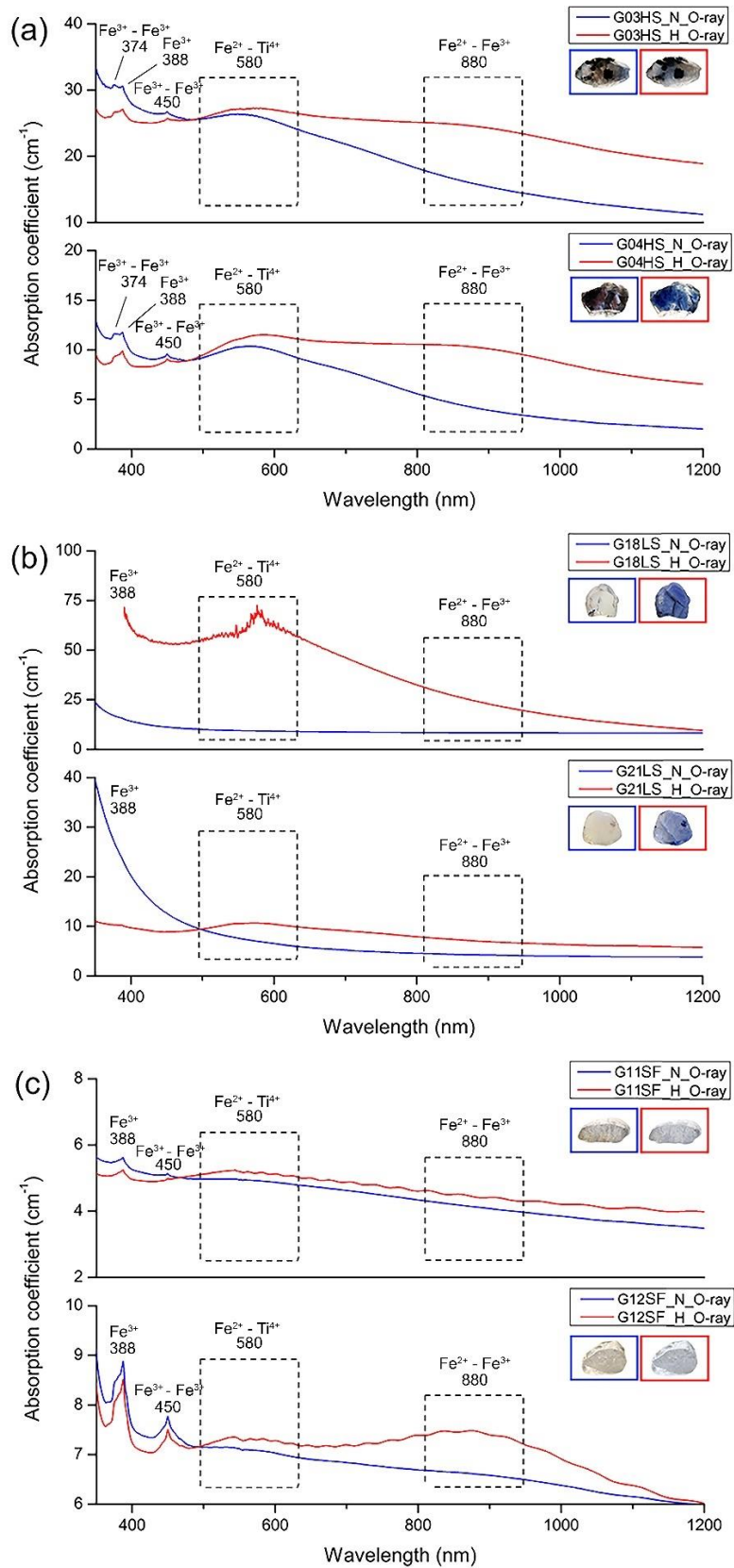
Figure 5. Optical absorption spectra of untreated (blue lines) and heated (red lines) samples: **(a)** HS group (G03HS, G04HS); **(b)** LS group (G18LS, G21LS); **(c)** SF group (G11SF, G12SF). Sizes of stones range between 4 and 12 mm.

217 Spectral characteristics of corundum containing Fe^{3+} ions exhibit a high degree of

218 complexity. It is noteworthy that Fe^{3+} has electron configuration d^5 resulting in a crystal field spectrum

219 with ground state $^6A_1$ (Ferguson and Fielding, 1972). Small peaks at 374 nm ($^4E^b$) and 450 nm ($^4A_1,^4E^a$)

220 should be attributed to the enhanced absorption of Fe^{3+}–Fe^{3+} pairs (McClure, 1962; Ferguson and Fielding,

221 1971; Krebs and Maisch, 1971; Ferguson and Fielding, 1972) as well as a weak broadband absorption at

222 540 nm ($^4T_2$) which could not be seen in this work. The distinct peak observed at a wavelength of 388 nm

223 ($^4T_2{}^b$) (Krebs and Maisch, 1971) is linked to the individual Fe^{3+} ions. This, however, does not rule out the

224 possibility of a higher-order cluster with extra ions or other point defects (Emmett et al., 2003).

225 Additionally, there is also a broad band at a wavelength of 330 nm ($^4T_1{}^b$) which is interpreted as a Fe^{3+}–

226 Fe^{3+} pair absorption (Ferguson and Fielding, 1972). As they are in low concentration (traces), this is also

227 present in the spectra of heated samples G03HS and G04HS, as well as in all spectra of sample G12SF in

228 this study. In trace contents both Fe^{2+} (d^6) and Ti^{4+} (d^0) ions alone do not exhibit any absorption in corundum

229 in the visible range (Townsend, 1968); on the other hand, Fe^{2+}–Ti^{4+} pairs ($t_2 \rightarrow {}^2E$) (Ferguson and Fielding,

230 1971) may yield a broad band absorption around 580 nm (E⊥c), or 700 nm (E∥c) (Dubinsky et al., 2020).

231 The Fe^{2+}–Fe^{3+} pair gives rise to the broad absorption band at ca. 880 nm (Fig. 5; Ferguson and Fielding,

232 1972).

233

234 **3.5 FTIR spectroscopy**

235 FTIR spectra of most samples yielded identical patterns within the range of 1600–4000 cm^{-1} (Fig. 6). They

236 usually showed CO_2 peaks (at 2339 and 2360 cm^{-1}), as well as C–H stretching related peaks (at 2856 and

237 2925 cm^{-1}), likely from artefacts (Fig. 6, blue lines), in accordance with Hughes (2017) and

238 Soonthorntantikul et al. (2021). However, O–H stretching of boehmite/diaspore peaks (at 1975 and 2105

239 cm^{-1}) (Delattre et al., 2012; Sun et al., 2015; Choi et al., 2017; Filatova et al., 2021; Soonthorntantikul et

240 al., 2021) was only observed in sample G03HS (Fig. 7a, blue line). Weak absorption features of O–H

241 stretching from H_2O (broad band at ca. 3400 cm^{-1}) and OH groups (ca. 3600–3700 cm^{-1}) were only found

242 in the untreated samples (blue lines), see Fig. 6a.

243

244
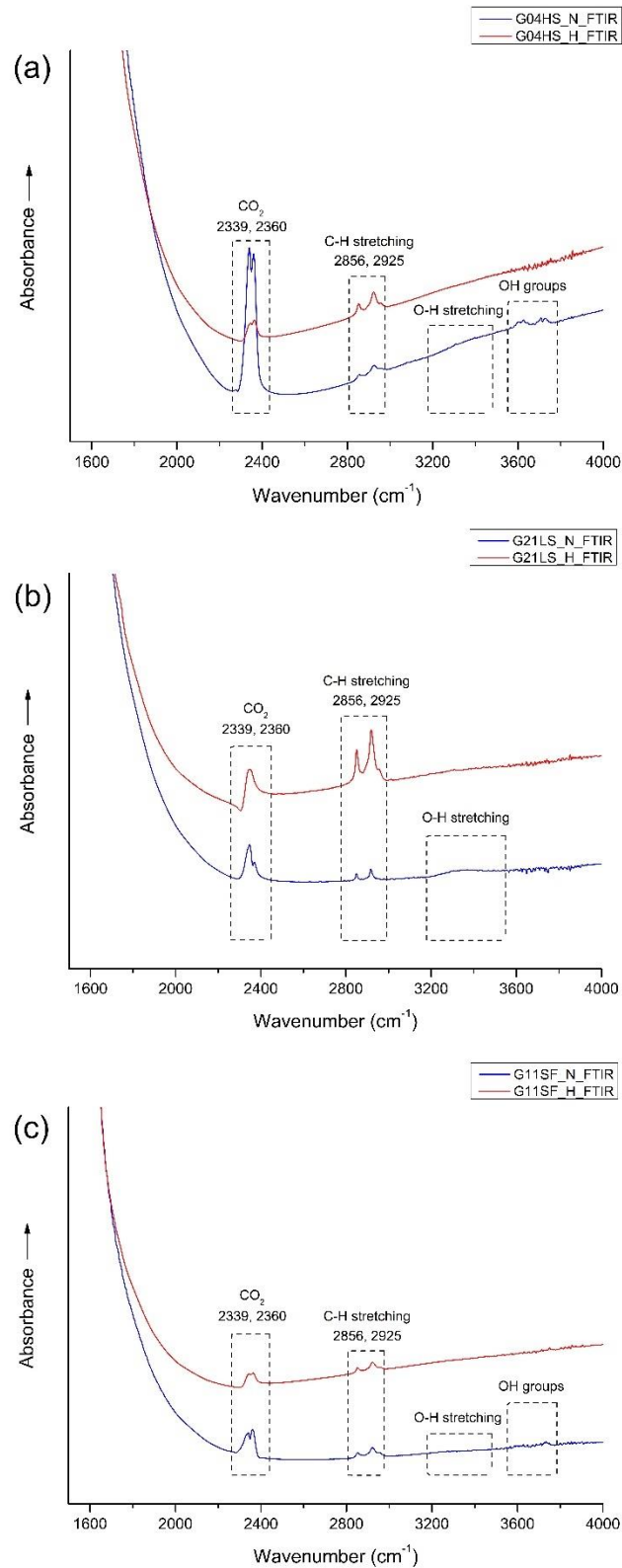
Figure 6. FTIR spectra obtained before (blue lines) and after (red lines) heating experiments of representative samples G04HS **(a)**, G21LS **(b)**, and G11SF **(c)**, respectively.

247

248   After heating, boehmite/diaspore–related absorption peaks (only observed in sample

249   G03HS, Fig. 7a) at 1975 and 2105 cm^{-1} disappeared. In contrast, the 3309 cm^{-1} hydroxyl (O–H) absorption,

250   which was not present in any natural sample before heating, appeared only in sample G18LS after heating

251   (Fig. 7b, red line).

252
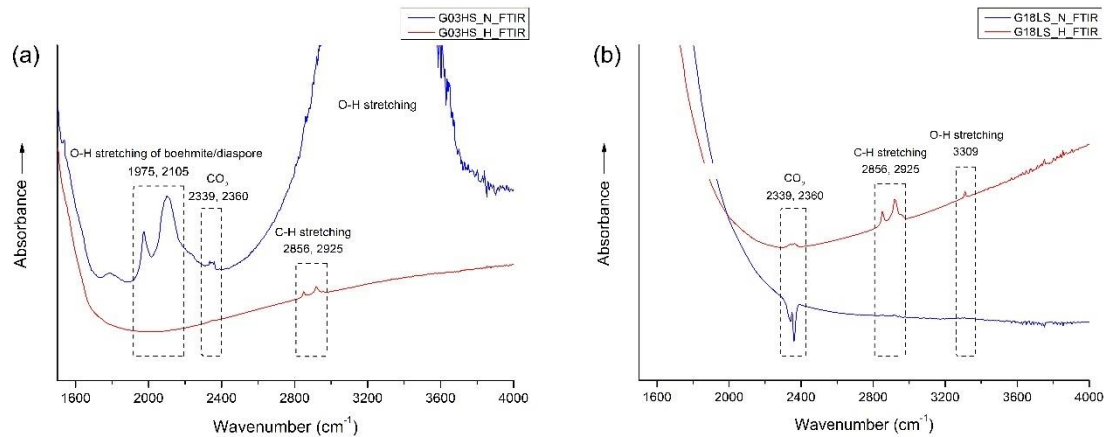
253

254   **Figure 7.** FTIR spectra obtained before (blue lines) and after (red lines) heat treatment of samples G03HS

255   **(a)** and G18LS **(b)**.

256

257   In this study, the non-systematic occurrence of O–H absorption in the 3100–3600 cm^{-1}

258   range in all natural geuda sapphire samples, together with the development of a weak absorption at 3309

259   cm^{-1} upon heating in only one of the samples (see Fig. 7b, red line), address the limitation to differentiate

260   unheated and heated sapphire by FTIR spectroscopy. Furthermore, heat treatment employed in this study

261   did not involve the use of any additional gases, such as hydrogen, to create a reducing atmosphere within

262   the furnace. Despite this, the 3309 cm^{-1} absorption band was seen after the heating process. This might be

263   in accordance with an explanation proposed earlier by Notari et al. (2018).

264   The controversy of the presence of an O–H peak in the FTIR spectrum in unheated and

265   heated sapphire could be attributed to an inherent hydrogen content of the corundum. Hydrogen was found

266   in corundum, primarily in the form of alumina hydrates (Notari et al., 2018). These hydrates could release

267   hydrogen through de–hydroxylation at temperatures as low as approx.approx. 450 °C. Additionally,

268   hydrogen was present in the air as H_2O, which can be split at temperatures around 900 °C to produce

269   hydrogen gas (H_2) and oxygen gas (O_2) through the reaction $2H_2O \rightarrow 2H_2 + O_2$ (Notari et al., 2018).

270

271   **3.6 Photoluminescence imaging and spectroscopy**

272   Photos presenting luminescence of some samples both before and after heat treatment are shown in Fig. 8.

273   Before heating, all natural sapphire samples were inert to SWUV light; moreover, all LS and SF samples

274   exhibited orange to red luminescence under LWUV light (Fig. 8). After heating, all LS and SF samples,

275   exhibited intense blue luminescence under SWUV light whereas their initial orange to red luminescence

276   under LWUV light turned into a strong purplish red luminescence (Fig. 8, samples G06LS and G20LS in

277   particular). In summary, the HS samples were all inert to SWUV and LWUV light both before and after

278 heating. Notably under LWUV light, an initial orange to red luminescence of a few samples from the SF
279 group was drastically reduced after heating (e.g., G23SF in Fig.8).

280

Samples		Unheated			Heated		
		White light (LED)	LWUV (365 nm)	SWUV (225 nm)	White light (LED)	LWUV (365 nm)	SWUV (225 nm)
High-density-silk (HS)	G01HS						
	G02HS						
Low-density-silk (LS)	G06LS						
	G20LS						
Silk-free (SF)	G14SF						
	G23SF						
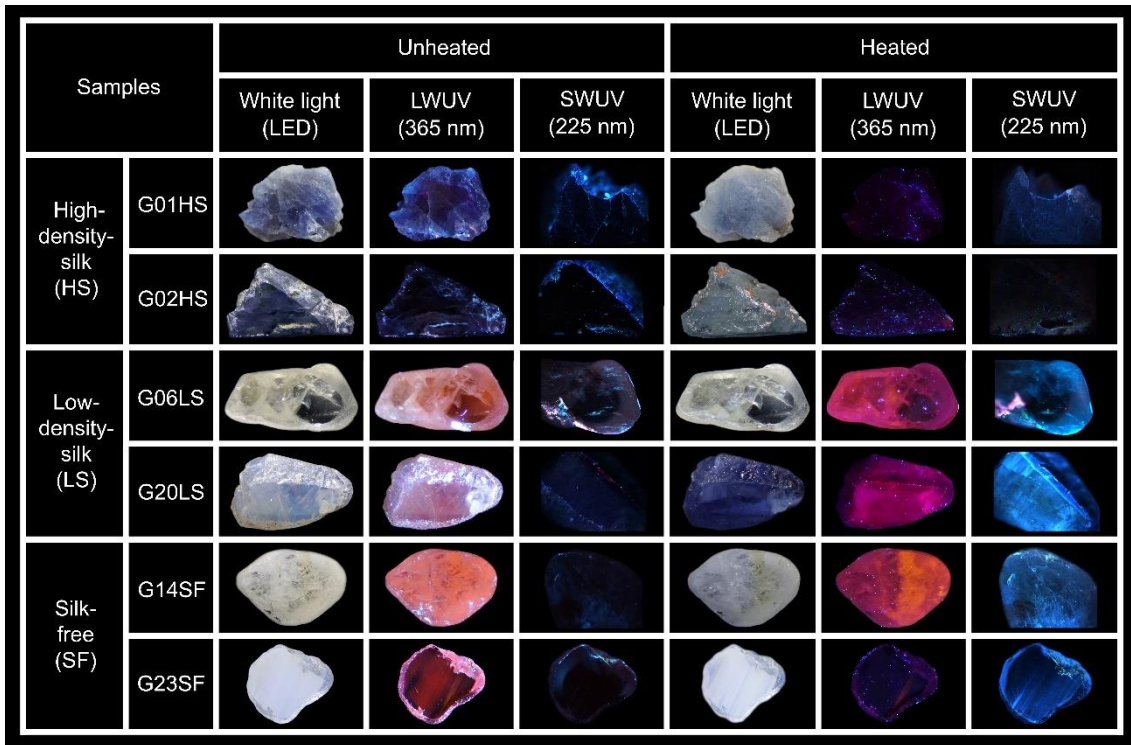
281
282 **Figure 8.** Representative images of HS (G01HS, G02HS), LS (G06LS, G20LS), and SF (G14SF, G23SF)
283 groups obtained under LWUV and SWUV illumination before and after heating. Sizes of stones range
284 between 4 mm and 12 mm.

285

286 The UV–excited PLspectra showed that all the unheated and heated sapphire samples
287 have an identical feature of two narrow peaks of trace Cr^{3+} lines at around 692.8 and 694.2 nm (Fig. 9) that
288 are assigned to the spin–forbidden $^2E \rightarrow {}^4A_2$ relaxation of trace Cr^{3+} (Nelson and Sturge, 1965). However,
289 the Cr^{3+} lines of some samples (Fig. 9c) are too weak to be visible within the noise of a broad and strong
290 emission band. All unheated sapphire samples showed a similar emission band in the orange to red region
291 centered around 630–650 nm (Fig. 9a–c, blue line). Remarkably, this appears to be associated with orange
292 to red luminescence under LWUV light, as noted by (Segura, 2013; Vigier et al., 2021a, b, c; Vigier and
293 Fritsch, 2022). Despite having the emission band around 630–650 nm, only unheated sapphire from HS
294 group appeared inert under LWUV illumination while the others revealed orange to red luminescence.

295 After heating, significant alteration in the emission band was observed, as depicted by
296 the red lines in Fig. 9a–c. The PL spectra of sample G03HS exhibited a notable reduction in the emission
297 band through the visible region (Fig. 9a, red line). This went along with a lack of luminescence both under
298 SWUV and LWUV excitation, whereas sample G12SF demonstrated a slight increase of the emission band
299 in the orange to red region (Fig. 9c, red line). More details are given in the discussion part below.

300 In contrast to the other groups, after heating, sample G21LS (Fig. 9b, red line) exhibited
301 a significant emission band in the green region at around 525 nm. Note that this broad emission is excited
302 with the 325 nm laser (Fig. 9) but does not seem to affect significantly the emission colors observed under

303 SWUV (225 nm) and LWUV (365 nm) excitation (Fig. 8). For a discussion of the possibly strong

304 dependence of emission intensity (and color) on the excitation wavelength see for instance Zeug et al.

305 (2022). Likewise heated sapphire has been proposed to have an emission band in the blue region, which

306 corresponds to blue luminescence under SWUV light (Nassau, 1981; Hughes, 2017; Vigier et al., 2023).

307
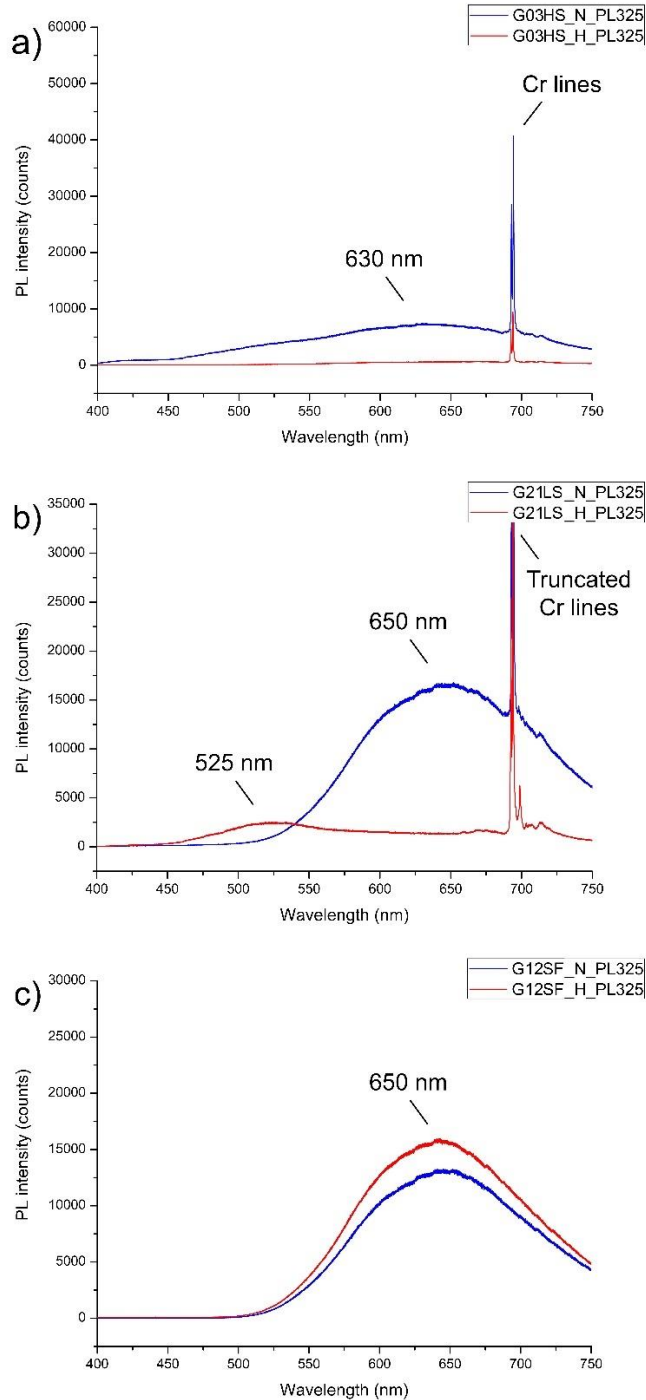
308

309 **Figure 9.** Representative PL (UV–excited) spectra obtained before (blue lines) and after (red lines) heating

310 of sample G03HS **(a)**, sample G21LS **(b)**, and sample G12SF **(c)**.

311

312 **4 Discussion**

313

314 **4.1 Generalities**

315 After Ti^{4+} ions are being exposed to SWUV light, they yield luminescence (Nasdala and Fritsch, 2024).

316 However, blue luminescence was not observed in both unheated and heated basaltic sapphire, possibly due

317 to the abundant presence of Fe^{2+} of basaltic origin that may strongly quench such blue luminescence

318 (Soonthorntantikul et al., 2019). More details will be discussed in this report. Furthermore, even though

319 microscopic inclusions have been the distinguishing characteristics of heated sapphire, identifying heat–

320 treated sapphire remains challenging (Crowningshield, 1966; Hughes, 2017). FTIR spectroscopy has also

321 been applied to detect heated sapphire. In some cases, the presence or absence of specific FTIR features in

322 the O–H absorption region (3100–3600 cm^{-1}) may serve as an indicator of heat treatment (Smith, 1995;

323 Beran and Rossman, 2006; Saeseaw et al., 2018); however, it is probably not a conclusive evidence

324 (Ediriweera and Perera, 1989; Perera, 1993; Sutthirat et al., 2006; Cartier, 2009; Jaliya et al., 2020). For

325 example, the presence of the 3309 cm^{-1} FTIR absorption peak was used as an indicator of heated corundum

326 (Hughes and Perkins, 2019; Soonthorntantikul et al., 2021). However, recent discoveries show that this

327 peak may also be found in unheated sapphire, suggesting that it is not a reliable indication of heat treatment

328 (Hughes, 1997, 2017; Hughes and Perkins, 2019; Soonthorntantikul et al., 2021).

329

330 **4.2 Silk inclusions and coloration of sapphire**

331 Studies addressing brown silk inclusions in corundum are scarce. Soonthorntantikul et al. (2021) reported

332 a mix of whitish silk and irregular/flaky/platelet–like brownish silk inclusions in corundum from Mogok.

333 Brown silk was ascribed as presumable ilmenite ($FeTiO_3$) which is noticeable in high–Fe sapphire, whereas

334 white silk was suggested to consist of rutile (TiO_2). The brown silks seen in our sapphire samples are likely

335 ilmenite, which is supported by their irregular/flaky/platelet–like brownish appearance and their high Fe

336 and Ti contents (note that the highest quantity of Fe was found in the HS group). Ilmenite decomposition

337 upon heat treatment does result in Fe and Ti migration into the host sapphire and subsequently causes blue

338 coloration. In particular, the decomposition of brown silks during heat treatment induces the formation of

339 blue dots, which is a result of the Fe^{2+}–Ti^{4+} pairing formation. Upon closer inspection using a high–

340 resolution microscope, these blue dots reveal distinct micro–inclusions as melt inclusions (with size of ≤ 1

341 μm, see Fig. 4), which have never been documented before. However, it should be noted that these melt

342 inclusions are possibly derived from the decomposition of silks.

343 This work focuses only on blue coloration in sapphire which mainly relates to the Fe^{2+}–

344 Ti^{4+} pair, as initially noted by Townsend (1968), followed by Mattson and Rossman (1988), Moon and

345 Phillips (1994), and Emmett et al. (2003). Ti exhibits electron–donor properties, whereas Fe may function

346 as an electron acceptor. When occupying neighboring Al^{3+} positions, absorption due to intervalence charge

347 transfer between such donor-acceptor pairs may occur (details reported by Emmett et al., 2003 and

348 Monarumit et al., 2023).

349 It should also be mentioned that Ti^{4+} ions do not exhibit any absorption characteristics in

350 the visible spectrum when considered individually. The Ti^{4+} ion has a closed–shell electron configuration,

351   whereas the Fe^{2+} ion mainly absorbs wavelengths within the near infrared and low–energy visible regions.

352   In contrast, when Fe^{2+} and Ti^{4+} ions are situated on neighboring structural sites, notable absorption bands

353   develop across the visible and near–infrared spectral regions. These Fe^{2+}–Ti^{4+} pairs exhibit a band center at

354   around 580 nm (see Fig. 5) when the electric field vector E is perpendicular to the crystallographic c–axis

355   (E⊥c), but a peak at 700 nm is seen when the electric field vector E is parallel to the crystallographic c–axis

356   (E∥c) (Dubinsky et al., 2020). Although the theory of the energy levels of an individual transition metal ion

357   inside a crystal has been extensively explored, the corresponding theory for ion pairs or clusters within a

358   crystal remains underdeveloped (Dubinsky et al., 2020).

359   In the present study, the natural unheated geuda sapphire samples were placed in

360   atmospheric conditions and subjected to a maximum temperature of 1650 °C for a duration of 10 h.

361   According to the examples presented in Fig. 1, samples G03HS and G04HS exhibited a noticeable increase

362   in blue coloration, particularly around the area of brown silks and brown color banding/zoning, after

363   heating. On the other hand, the initial blue patch (e.g. samples G01HS and G02HS) became paler blue after

364   heating, which might be due to the breakage of initial Fe–Ti pairs in those areas. The other groups, which

365   have yellowish and/or milky appearances, revealed an increase in blue color after heating (samples G12SF

366   and G18LS, Fig. 1). This blue coloration is attributed to two distinct factors, notably the decomposition of

367   silk inclusions and a subsequent charge transfer mechanism (Emmett and Douthit, 1993; Hughes, 1997,

368   2017; Nassau, 1980, 1981; Themelis, 2018). The process of charge transfer (Ferguson and Fielding, 1972;

369   Nassau, 1981) is described as:

$$Fe^{2+} + Ti^{4+} \rightleftarrows Fe^{3+} + Ti^{3+} \tag{1}$$
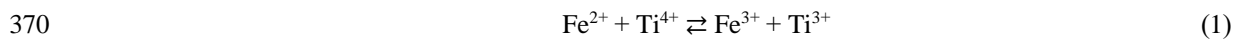
371   It is important to note that the blue color observed in sapphire could also be produced

372   with the application of heat in oxidizing conditions at high temperature. Heat treatment can be classified as

373   high– or low–temperature according to the decomposition of rutile silks in corundum (Nassau, 1981;

374   Emmett and Douthit, 1993; Emmett et al., 2003; Hughes, 2017; Hughes and Perkins, 2019). The term low–

375   temperature heat treatment has been used (typically referred to as below 1000 °C) when rutile particles still

376   reveal their original structures. On the other hand, temperatures beyond 1350 °C denote high–temperature

377   heat treatment when rutile silks start to decompose and dissolve within the corundum host (Hughes, 2017;

378   Themelis, 2018). Consequently, internal diffusion (indicated by a colored halo surrounding the crystal

379   inclusion), molten or altered inclusions, and/or broken silk are strong indicators of high–temperature heat

380   treatment. However, low–temperature heat treatment can also produce various altered mineral inclusions

381   (Kammerling et al., 1990; McClure and Smith, 2000; McClure et al., 2010; Pisutha–Arnond, 2017;

382   Soonthorntantikul et al., 2019).

383   In recent studies, the possibility of employing Fe^{2+}-Fe^{3+} charge transfer as an alternate

384   method for blue coloration has also been mentioned (Nikolskaya et al., 1978; Schmetzer and Kiefert, 1990;

385   Häger, 1992, 2001; Sripoonjan et al., 2014; Pisutha–Arnond, 2017). However, it is necessary to emphasize

386   that this approach was considered highly improbable (Nassau, 1981). Nevertheless, previous studies have

387   indicated that a minor proportion of geuda sapphire from Sri Lanka and geuda–like sapphire from Mogok

388   in Burma revealed an alteration in color to blue when subjected to heating in an oxidizing environment

389   (Hughes, 1997, 2017; Kyi et al., 1999), which is in complete contradiction to the treatment method

390   employed for the geuda sapphire in a reducing condition. The appearance of certain stones displaying a

391 blue coloration under oxidizing conditions might be attributed to the presence of ilmenite silks, which is

392 composed of Fe and Ti, with Fe in its reduced Fe^{2+} state (Hughes, 1997). Therefore, it is unnecessary to

393 reduce Fe^{3+} to Fe^{2+} ions to generate the Fe^{2+}–Ti^{4+} pairs that are responsible for the manifestation of the blue

394 color. Hence, the blue areas have a substantial concentration of Fe ions in form of Fe-Ti pairs, derived from

395 the decomposed ilmenite silk inclusions.

396 According to Nassau (1981) and Koivula (1987), the presence of blue dots in heated

397 sapphire is attributed to remains of dissolved silk inclusions and internal cation diffusion. The diffusion

398 process is positively correlated with temperature and duration of heat treatment (Nassau, 1981). Despite

399 the slow diffusion rates of Fe and Ti, the distances across are extremely short, i.e., just a few micrometers

400 (Nassau, 1981). Consequently, a potential Fe–Ti combination within the corundum's lattice may generate

401 the blue dots.

402 The presence of melt inclusions among the blue dots after high–temperature heating

403 might be due to the decomposition of brown silk and its solubility into the host sapphire as demonstrated

404 by Jung et al. (2009). They predicted a phase relationship within the Al_2O_3–Ti_2O_3–TiO_2 system based on

405 experimental data and thermodynamic calculation. Consequently, they suggested that a liquid phase (the

406 composition of the liquid inclusion phase varies significantly between Al_2O_3 and Ti_3O_5) could possibly be

407 present at a temperature of 1600 °C and slightly below, which is close to the heating temperature (1650 °C)

408 of our experiment. Silk inclusions as represented by Ti_2O_3–TiO_2 components may have dissolved into the

409 host sapphire (Al_2O_3 component), and produced a proper composition of solution which could be melted

410 partially at ≤ 1650 °C. Some of these melts can be preserved as inclusions after cooling down.

411

4.3 Luminescence of sapphire

413 Luminescence of corundum may be assigned to two types, namely (a) emissions of impurity–related centers

414 such as Ti^{4+} (commonly known) and (b) emissions of defect–related centers, which typically involve either

415 vacancies, such as oxygen (O) or aluminum (Al) vacancies known as F center (color center; from the

416 German "*Farbzentrum*"), or interstitials (Al_i and O_i), possibly trapped at impurities (less known), or both

417 (Viger et al., 2021a–c). This means that defect–related emission centers in corundum refer to an

418 inconsistency in the atomic arrangement limited to one or a few atoms (often called color–centers). O

419 vacancies (or electron holes) are sometimes called hole centers, because the holes simply designate the

420 absence of an electron. The holes are sometimes filled with one or two electrons in order to maintain

421 electroneutrality (Vigier et al., 2021a).

422 As presented in Fig. 8, a notable orange to red luminescence is easily noticeable under

423 LWUV excitation in most unheated sapphire samples, except for those of the HS group, which appear inert.

424 After heat treatment, the orange to red luminescence that is initially observed in all samples of the LS group

425 and many samples of the SF group turns into a purplish-red luminescence. In contrast, no orange to red or

426 purplish red luminescence is observed in any sample of the HS group both before and after heating.

427 The origin of orange to red luminescence in sapphire remained controversial, with

428 varying ideas among researchers (Vigier et al., 2021a, b, 2023). The occurrence of orange luminescence

429 has been documented in some previous studies (e.g. Spencer, 1927; Kane, 1982; Emmett et al., 2003;

430 Fritsch et al., 2003; Nasdala and Fritsch, 2024). In the beginning, it was hypothesized that this luminescence

431 is associated with the geographic origin of yellow sapphire from Sri Lanka (Webster, 1984). Subsequently,

432 Segura (2013) presented an alternative argument to this notion, suggesting the presence of orange

433 luminescence in various colors of corundum, regardless of treatment or synthetic origin, might be attributed

434 to the existence of some defects. However, the orange to red luminescence observed in our study

435 (characterized by a broad emission band) seems to be associated with complex defect–related centers.

436 Orange to red luminescence in sapphire is not due to impurities (Vigier et al., 2021a, b).

437 HS sapphire (e.g., with ilmenite, $FeTiO_3$) lack noticeable luminescence, likely because Fe^{2+} suppresses

438 luminescence, contrasting with LS and SF sapphire, which display stronger luminescence both before and

439 after heating. While sample G23SF shows decreased purplish–red luminescence after heating, most display

440 increased purplish–red luminescence, potentially due to complex, defect–related centers in the sapphire

441 lattice. Observations suggested that Fe^{2+} acts as a luminescence quencher in the orange to red range

442 (Andrade et al., 2008; Norrbo et al., 2016; Vigier et al., 2021a, b, c; Vigier and Fritsch, 2022); Orange

443 luminescence generally appears in colorless, low–Fe areas (Segura, 2013; Notari et al., 2003). However, a

444 definitive explanation remains unresolved. Regarding blue luminescence, it has been observed that upon

445 exposure to SWUV light, all natural unheated samples appeared inert. After heating, apart from HS

446 sapphire, a distinct blue luminescence has been detected throughout most heated sapphire samples (Fig. 8).

447 Previous studies suggest that luminescence in sapphire becomes noticeable only at heating temperatures of

448 1000 °C (Hughes and Perkins, 2019), at which point blue luminescence is linked to heat treatment detection.

449 This luminescence is believed to arise from silk inclusions composed of TiO_2, commonly found in natural

450 blue sapphire. Notably, despite the relatively low Ti concentration (0.02–0.03 wt% oxide) in comparison

451 to Fe (0.05–0.08 wt% oxide) in some samples (e.g., G12SF and G21LS), blue luminescence remains

452 detectable. In contrast, HS samples (e.g., G02HS) show an absence of blue luminescence, likely due to the

453 presence of ilmenite, supporting findings by Norrbo et al. (2016), Andrade et al. (2008), as well as Vigier

454 et al. (2021a–c; 2023) that Fe^{2+} acts as a luminescence quencher. Blue luminescence has been associated

455 with the interaction between O^{2-} and Ti^{4+} ions (Evans, 1994; Wong et al., 1995b; Nasdala and Fritsch,

456 2024), followed by a later hypothesis of a charge transfer process involving Ti^{4+} ions and certain defect–

457 related centers (Lacovara et al., 1985; Mikhailik et al., 2005). However, it was widely accepted that the

458 blue luminescence (characterized by a broad emission band at blue to green region) observed in sapphire

459 under SWUV illumination is associated with the presence of Ti impurities, which are classified as element–

460 related defects (Vigier et al., 2021a, b). Thus, it is likely that the blue luminescence reported in this work

461 is associated with Ti impurities, whereas orange to red luminescence seems to be associated with complex

462 defect–related emission centers.

463 The correlation between the orange to red PL emission band (approx. 650 nm, Fig. 9 blue

464 lines) and orange to red luminescence in unheated sapphire (Fig. 8), as well as the emission band (approx.

465 525 nm, Fig. 9 red lines) and blue luminescence in heated sapphire (Fig. 8), is particularly evident in the

466 LS group (Fig. 9b). In contrast, the HS group shows a reduction in emission across the visible spectrum

467 after heating, indicating inertness under LWUV and SWUV excitation (Fig. 9a). The SF group exhibits a

468 notable increase in the red emission band (Fig. 9c) and intense purplish–red luminescence under LWUV

469 excitation after heating. Interestingly, this group also displays strong blue luminescence under SWUV

470 excitation despite the absence of a corresponding blue emission band, likely due to the 325 nm excitation

471 laser used in our PL investigation. Variations in excitation wavelengths significantly affect observed
472 emissions, as noted by Wong et al. (1995a) and Vigier et al. (2023), who showed that their sapphire
473 emission band at 425 nm was only visible with a 254 nm excitation laser. Utilizing distinct SWUV (225
474 nm) and LWUV (365 nm) lasers, or conducting excitation spectroscopy, may yield more accurate results
475 compared to relying solely on a 325 nm laser. Thus, the presence of orange to red luminescence at approx.
476 650 nm and blue luminescence at around 525 nm are vital indicators for differentiating unheated and heated
477 sapphire.
478

479 **5 Conclusions**

480 The present study demonstrates that melt inclusions (~1 µm) serve as indicators of heat treatment in
481 sapphires, and highlights the critical role of luminescence in distinguishing unheated from heated geuda
482 sapphire. Under LWUV light, orange luminescence may arise from defect–related F centers, while blue
483 luminescence under SWUV light likely correlates with Ti impurities. Geuda sapphires with low Fe
484 concentrations exhibit distinct luminescence, whereas those with HS inclusions show minimal
485 luminescence due to Fe^{2+} quenching effects. The presence of orange luminescence may be a helpful
486 indicator for unheated geuda sapphires, while blue luminescence is generally absent in unheated samples,
487 confirming its utility for identifying heated geuda sapphire. Although the 3309 cm^{-1} O–H stretching band
488 from FTIR analysis alone is insufficient for differentiation, increased intensity around the 580 nm of an
489 optical spectra effectively indicates heat treatment, as it corresponds to higher Fe–Ti pair concentrations
490 from silk inclusion decomposition. Combining blue and/or purplish–red luminescence with additional
491 analytical techniques provides a promising strategy for accurately distinguishing between unheated and
492 heated geuda sapphires (Fig. 10). Future research should acquire emission and excitation spectra on the
493 samples before and after heat treatment. Further investigation of luminescence characteristics from various
494 sapphire origins (and colors) and clarify the specific Fe and Ti concentrations impacting luminescence is
495 also recommended. Finally, using as low as 200–254 nm laser excitation may enhance the detection of
496 emission shifts towards the blue region in heated sapphires, improving gemological identification criteria.
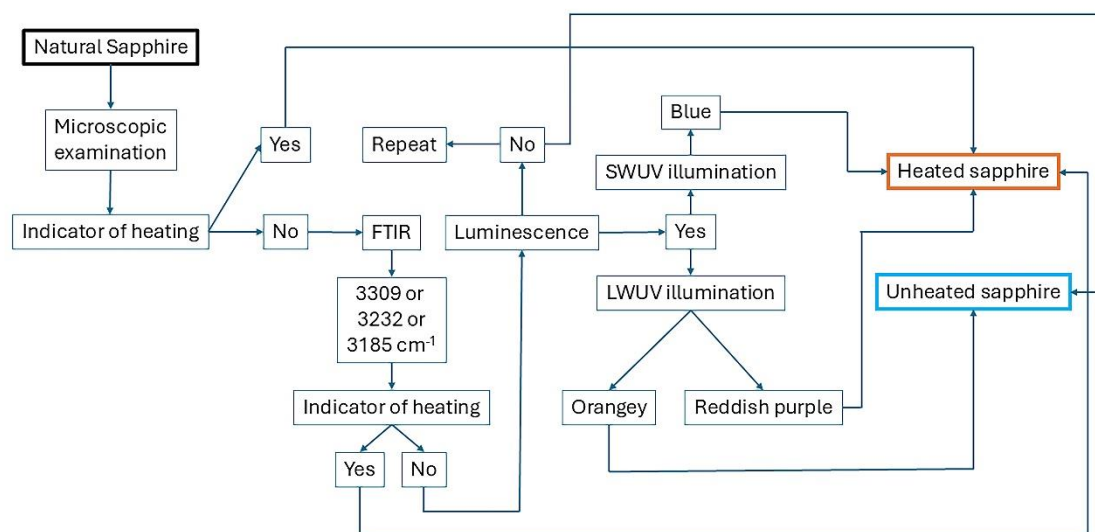
Figure 10. Flowchart proposing the combined strategy for heated sapphire identification criteria.

Author contributions. T.P., C.S., B.W., L.N. conducted conceptualization, E.G.Z. acquired samples, T.P., C.S., B.W., L.N., C.C.N., M.W., E.L., G.G., T.S. conducted analyses and evaluation, T.P. wrote the manuscript, all co–authors reviewed and edited the manuscript.

6 References

Alombert–Goget, G., Li, H., Guyot, Y., Brenier, A., and Lebbou, K.: Luminescence and coloration of undoped and Ti–doped sapphire crystals grown by Czochralski technique, J. Lumin., 169, 516–519, https://doi.org/10.1016/j.jlumin.2015.02.001, 2016a.

524   Alombert-Goget, G., Li, H., Faria, J., Labor, S., Guignier, D., and Lebbou, K.: Titanium distribution in

525   Ti-sapphire single crystals grown by Czochralski and Verneuil technique, Opt. Mater., 51, 1-4,

526   https://doi.org/10.1016/j.optmat.2015.11.016, 2016b.

527   Andrade, L. H. C., Lima, S. M., Novatski, A., Neto, A. M., Bento, A. C., Baesso, M. L., Gandra, F. C. G.,

528   Guyot, Y., and Boulon, G.: Spectroscopic assignments of Ti^{3+} and Ti^{4+} in titanium-doped OH-free

529   low silica calcium aluminosilicate glass and role of structural defects on the observed long lifetime

530   and high fluorescence of Ti^{3+} ions, Phys. Rev. B, 78, 224202,

531   https://doi.org/10.1103/PhysRevB.78.224202, 2008

532   Beran, A. and Rossman, G. R.: OH in naturally occurring corundum, Eur. J. Mineral., 18, 441-447,

533   https://doi.org/10.1127/0935-1221/2006/0018-0441, 2006.

534   Cartier, L. E.: Ruby and sapphire from marosely, Madagascar, J. Gemmol., 31, 171-180,

535   http://doi.org/10.15506/JoG.2009.31.5.171, 2009.

536   Choi, E., Song, K., An, S., Lee, K., Youn, M., Park, K., Jeong, S., and Kim, H.: Cu/ZnO/AlOOH catalyst

537   for methanol synthesis through CO_2 hydrogenation, Korean J. Chem. Eng., 35, 73–81,

538   https://doi.org/10.1007/s11814–017–0230–y, 2018.

539   Crowningshield, R.: Developments and highlights at the gem trade lab in new york: Unusual items

540   encountered (sapphire with unusual fluorescence), Gems Gemol., 12, 73, 1966.

541   Crowningshield, R.: Developments and highlights at GIA's lab in New York: Unusual fluorescence,

542   Gems Gemol., 13, 120-122, 1970.

543   Delattre, S., Balan, E., Lazzeri, M., Blanchard, M., Guillaumet, M., Beyssac, O., Haussühl, E., Winkler,

544   B., Salje, E. K. H., and Calas, G.: Experimental and theoretical study of the vibrational properties

545   of diaspore (α–AlOOH), Phys. Chem. Miner, 39, 93–102, https://doi.org/10.1007/s00269–011–

546   0464–x, 2012.

547   Dubinsky, E. V., Stone-Sundberg, J., and Emmett, J. L.: A quantitative description of the causes of color

548   in corundum, Gems Gemol., 56, 2-28, https://doi.org/10.5741/gems.56.1.2, 2020.

549   Ediriweera, R. and Perera, S.: Heat treatment of geuda stones – spectral investigation, J. Gemmol., 21,

550   403-410, https://doi.org/10.15506/jog.1989.21.7.403, 1989.

551   Emmett, J. L. and Douthit, T. R.: Heat treating the sapphires of Rock Creek, Montana, Gems Gemol., 29,

552   250-272, https://doi.org/10.5741/gems.29.4.250, 1993.

553   Emmett, J. L., Scarratt, K., McClure, S. F., Moses, T., Douthit, T. R., Hughes, R., Novak, S., Shigley, J.

554   E., Wang, W., Bordelon, O., and Kane, R. E.: Beryllium diffusion of ruby and sapphire, Gems

555   Gemol., 39, 84–135, https://doi.org/10.5741/gems.39.2.84, 2003.

556   Evans, B. D.: Ubiquitous blue luminescence from undoped synthetic sapphire, J. Lumin., 60-61, 620-626,

557   https://doi.org/10.1016/0022-2313(94)90233-X, 1994.

558   Ferguson, J. and Fielding, P. E.: The origins of the colors of yellow, green and blue sapphires, Chem.

559   Phys. Lett., 10, 262-265, https://doi.org/10.1016/0009-2614(71)80282-8, 1971.

560   Ferguson, J. and Fielding, P. E.: The origins of the colors of natural yellow, blue, and green sapphires,

561   Aust. J. Chem., 25, 1371-1385, https://doi.org/10.1071/CH9721371, 1972.

562 Filatova, N. V., Kosenko, N. F., and Artyushin, A. S.: The physicochemical analysis of bayerite $Al(OH)_3$
563      $\rightarrow \gamma$–Al_2O_3 transformation, J. Sib. Fed. Univ. Chem., 14, 527–538, https://doi.org/10.17516/1998–
564   2836–0260, 2021.

565 Fritsch, E., Chalain, J. P., Hanni, H., Devouard, B., Chazot, G., Giuliani, G., Schwartz, D., Rollion-Bard,
566   C., Garnier, V., Barda, S., Ohnenstetter, D., Notari, F., and Maitrallet, P.: Le nouveau traitement
567   produisant des couleurs orange a jaune dans les saphirs, Revue de Gemmologie n° 147-Février
568   2003, 147, 11-23, 2003.

569 Häger, T.: Farbgebende und "farbhemmende" Spurenelemente in blauen Saphiren, Berichte der
570   Deutschen Mineralogischen Gesellschaft – Beih. Eur. J. Mineral., 4, 109, 1992.

571 Häger, T.: High temperature treatment of natural corundum, in: Proceeding of the International Workshop
572   on Material Characterization by Solid State Spectroscopy: The Minerals of Vietnam, Hanoi, 4–10
573   April 2001, 1-10, 2001.

574 Hughes, E. B. and Perkins, R.: Madagascar sapphire: Low temperature heat treatment experiments, Gems
575   Gemol., 55, 184-197, http://doi.org/10.5741/GEMS.55.2.184, 2019.

576 Hughes, R. W. (1st edn.): Ruby & Sapphire, RWH Publishing, 511 pp., ISBN 0964509768, 1997.

577 Hughes, R. W.: Ruby & sapphire: A gemologist's guide, RWH Publishing/Lotus Publishing, 816 pp.,
578   ISBN 9780964509719, 2017.

579 Jaliya, R. G. C., Dharmaratne, P. G. R., and Wijesekara, K. B.: Characterization of heat treated geuda
580   gemstones for different furnace conditions using FTIR, XRD and UV–Visible spectroscopy
581   methods, Solid Earth Sci., 5, 282-289, https://doi.org/10.1016/j.sesci.2020.11.001, 2020.

582 Jung, I. H., Eriksson, G., Wu, P., and Pelton, A.: Thermodynamic modeling of the Al_2O_3–Ti_2O_3–TiO_2
583   system and its applications to the Fe–Al–Ti–O inclusion diagram, ISIJ INT., 49, 1290–1297,
584   https://doi.org/10.2355/isijinternational.49.1290, 2009.

585 Kammerling, R. C., Koivular, J. I., and Kane, R. E.: Gemstone enhancement and its detection in the
586   1980s, Gems Gemol., 26, 32-49, https://doi.org/10.5741/GEMS.26.1.32, 1990.

587 Kane, R. E.: The gemological properties of Chatham flux-grown synthetic orange sapphire and synthetic
588   blue sapphire, Gems Gemol., 18, 140-153, https://doi.org/10.5741/GEMS.18.3.140, 1982.

589 Krebs, J. J. and Maisch, W. G.: Exchange effects in the optical-absorption spectrum of Fe^{3+} in Al_2O_3,
590   Phys. Rev. B, 4, 757-769, https://doi.org/10.1103/PhysRevB.4.757, 1971.

591 Kyi, U. H., Buchhol, P., and Wolf, D.: Heat treatment of milky sapphires from the Mogok stone tract,
592   Myanmar, J. Gemmol., 26, 313-315, https://doi.org/10.15506/jog.1999.26.5.313, 1999.

593 Lacovara, P., Esterowitz, L., and Kokta, M.: Growth, spectroscopy, and lasing of titanium-doped
594   sapphire, IEEE J. Quantum Electron., 21, 1614–1618, https://doi.org/10.1109/JQE.1985.1072563,
595   1985.

596 Mattson, S. M. and Rossman, G. R.: Fe^{2+}–Ti^{4+} charge transfer in stoichiometric Fe^{2+},Ti^{4+}–minerals, Phys.
597   Chem. Miner., 16, 78–82, https://doi.org/10.1007/BF00201333, 1988.

598 McClure, D. S.: Optical spectra of transition–metal ions in corundum, J. Chem. Phys., 36, 2757–2779,
599   https://doi.org/10.1063/1.1732364, 1962.

600 McClure, S. F. and Smith, C. P.: Gemstone enhancement and detection in the 1990s, Gems Gemol., 36,
601   336–539, http://doi.org/10.5741/GEMS.36.4.336, 2000.

602 McClure, S. F., Kane, R. E., and Sturman, N.: Gemstone enhancement and detection in the 2000s, Gems
603   Gemol., 46, 218–240, http://doi.org/10.5741/GEMS.46.3.218, 2010.

604 Mikhailik, V. B., Kraus, H., Wahl, D., and Mykhaylyk, M. S.: Luminescence studies of Ti-doped Al_2O_3
605   using vacuum ultraviolet synchrotron radiation., Appl. Phys. Lett., 86, 101909,
606   http://doi.org/10.1063/1.1880451, 2005.

607 Monarumit, N., Lhuaamporn, T., Wathanakul, P., Saiyasombat, C., and Wongkokua, W.: The acceptor–
608   donor pair recombination of beryllium–treated sapphires, Radiat. Phys. Chem., 206, 110756,
609   https://doi.org/10.1016/j.radphyschem.2023.110756, 2023.

610 Moon, A. R. and Phillips, M. R.: Defect clustering and color in Fe,Ti: α-Al_2O_3, J. Am. Ceram. Soc., 77,
611   356–367, https://doi.org/10.1111/j.1151–2916.1994.tb07003.x, 1994.

612 Nasdala, L., and Fritsch, E.: Luminescence: The "Cold Glow" of Minerals, Elements, 20, 287–292,
613   https://doi.org/10.2138/gselements.20.5.287, 2024.

614 Nassau, K.: The causes of color, Sci. Am., 243, 124–154,
615   https://doi.org/10.1038/SCIENTIFICAMERICAN1080-124, 1980.

616 Nassau, K.: Heat treating ruby and sapphire: Technical aspects, Gems Gemol., 17, 121–131,
617   https://doi.org/10.5741/GEMS.17.3.121, 1981.

618 Nelson, D. F. and Sturge, M. D.: Relation between absorption and emission in the region of the R lines of
619   ruby, Phys. Rev., 137, A1117–A1130, https://doi.org/10.1103/PhysRev.137.A1117, 1965.

620 Nikolskaya, L. V., Terekhova, V. M., and Samoilovich, M. I.: On the origin of natural sapphire color,
621   Phys. Chem. Miner., 3, 213–224, https://doi.org/10.1007/BF00633571, 1978.

622 Norrbo, I., Gluchowski, P., Hyppänen, I., Laihinen, T., Laukkanen, P., Mäkelä, J., Mamedov, F., Santos,
623   H. S., Sinkkonen, J., Tuomisto, M., Viinikanoja, A., and Lastusaari, M.: Mechanisms of
624   tenebrescence and persistent luminescence in synthetic hackmanite $Na_8Al_6Si_6O_{24}(Cl,S)_2$, ACS
625   Appl. Mater. Interfaces, 8, 11592–11602, https://doi.org/10.1021/acsami.6b01959, 2016.

626 Notari, F., Fritsch, E., and Grobon, C.: Comment l'observation de la luminescence (fuorescence) peut
627   aider a l'identification des corindons jaunes, rose orange et orange, traites par diffusion du
628   beryllium (How the observation of luminescence might aid in the identification of yellow, orangy
629   pink and orange corundum treated by Be-diffusion), Rev. de Gem., 148, 40–43, 2003.

630 Notari, F., Hainschwang, T., Caplan, C., and Ho, K.: The heat treatment of corundum at moderate
631   temperature, InColor, 42, 15–23, 2018.

632 Page, P. S., Dhabekar, B. S., Bhatt, B. C., Dhoble, A. R., and Godbole, S. V.: Role of Ti^{4+} in the
633   luminescence process of Al_2O_3:Si,Ti, J. Lumin., 130, 882–887,
634   https://doi.org/10.1016/j.jlumin.2009.12.029, 2010.

635 Palanza, V., Di Martino, D., Paleari, A., Spinolo, G., and Loredana, P.: Micro–Raman spectroscopy
636   applied to the study of inclusions within sapphire, J. Raman Spectrosc., 39, 1007–1011,
637   https://doi.org/10.1002/jrs.1939, 2008.

638 Palke, A. C., Saeseaw, S., Renfro, N. D., Sun, Z., and McClure, S. F.: Geographic origin determination of
639   blue sapphire, Gems Gemol., 55, 536-579, https://doi.org/10.5741/gems.55.4.536, 2019.

640 Peiris, B. P. S.: Color enhancement of diesal geuda, in: Proceedings of the National symposium on geuda
641   heat treatment, Sri Lanka, 10–11 June 1993, 113-122, 1993.

642 Perera, S. Z., Pannila, A. S., Gunasekera, H. P. N. J., and Ediriweera, R. N.: Anomalous behaviour of
643   certain geuda corundums during heat treatment, J. Gemmol., 22, 405–407,
644   https://doi.org/10.15506/jog.1991.22.7.405, 1991.

645 Perera, I.: Identification of treatable geuda by spectral investigations, in: Proceedings of the National
646   symposium on geuda heat treatment, Sri Lanka, 10–11 June 1993, 89-98, 1993

647 Pisutha-Arnond, V.: Ruby & sapphire treatments and identification: Decades of advancement, Amarin
648   Printing and Publishing, Bangkok, 96 pp., ISBN 978-6169145097, 2017.

649 Saeseaw, S., Kongsomart, B., Atikarnsakul, U., Khowpong, C., Vertriest, W., and Soonthorntantikul, W.:
650   Update on "low temperature" heat treatment of Mozambican ruby: A focus on inclusions and
651   FTIR spectroscopy. News from research, Gemological Institute of America, 37 pp., 2018.

652 Schmetzer, K. and Kiefert, L.: Spectroscopic evidence for heat treatment of blue sapphires from Sri
653   Lanka-additional data, J. Gemmol., 22, 80-82, 1990.

654 Segura, O.: La luminescence orange des corindons, Diplome Universitaire de Gemmologie de Nantes, 60
655   pp., 2013.

656 Smith, C. P.: A contribution to understanding the infrared spectra of rubies from Mong Hsu, Myanmar, J.
657   Gemmol., 24, 321-335, http://doi.org/10.15506/JoG.1995.24.5.321, 1995.

658 Soonthorntantikul, W., Khowpong, C., Atikarnsakul, U., Saeseaw, S., Sangsawong, S., Vertriest, W., and
659   Palke, A.: Observations on the heat treatment of basalt-related blue sapphires. News from
660   research, Gemological Institute of America, 60 pp., 2019.

661 Soonthorntantikul, W., Atikarnsakul, U., and Vertriest, W.: Blue sapphires from Mogok, Myanmar: A
662   gemological review, Gems Gemol., 57, 292-317, https://doi.org/10.5741/GEMS.57.4.292, 2021.

663 Soysa, E. S. K. and Fernando, W. S.: A field classification of low value corundum in Sri Lanka, J. Natn.
664   Sci. Coun. Sri Lanka, 20, 51-57, https://doi.org/10.4038/jnsfsr.v20i1.8058, 1992.

665 Spencer, L. J.: South African occurrences of willemite. Fluorescence of willemite and some other zinc
666   minerals in ultra-violet rays, Mineral. Mag., 21, 388–396,
667   https://doi.org/10.1180/minmag.1927.021.119.04, 1927.

668 Sripoonjan, T., Lhuaamporn, T., Nilhud, N., Sukkee, N., and Sutthirat, C.: Characteristics of Cyangugu
669   sapphire from rwanda, in: Proceedings of the 4th international gem and jewelry conference
670   (GIT2014) Chiang Mai, Thailand, 165-168, 2014.

671 Strange, L., Zhang, Y., Son, J., Gao, J., Joshi, V., and Yu, X. Y.: Aluminum hydroxide, bayerite,

672 boehmite, and gibbsite ToF–SIMS spectra in the negative ion mode. I. Surf. Sci. Spectra, 29,

673 025001. https://doi.org/10.1116/6.0001935, 2022.

674 Sun, T., Zhuo, Q., Chen, Y., and Wu, Z.: Synthesis of boehmite and its effect on flame retardancy of

675 epoxy resin, High Perform. Polym., 27, 1, 100–104, https://doi.org/10.1177/0954008314540312,

676 2015.

677 Sutthirat, C., Pattamalai, K., Sakkaravej, S., Pumpeng, S., Pisutha-Arnond, V., Wathanakul, P., Atichat,

678 W., and Sriprasert, B.: Indications of heating in corundum from experimental results, Gems

679 Gemol., 42, 86, 2006.

680 Themelis, T. (3rd edn.): The heat treatment of ruby & sapphire: Experiments & observations, Ted

681 Themelis, 294 pp., ISBN 0940965577, 2018.

682 Townsend, M. G.: Visible charge transfer band in blue sapphire, Solid State Commun., 6, 81-83,

683 https://doi.org/10.1016/0038-1098(68)90005-7, 1968.

684 Vertriest, W., Palke, A. C., and Renfro, N. D.: Field Gemology: Building a Research Collection and

685 Understanding the Development of Gem Deposits, Gems Gemol., 55, 491–494, 2019.

686 https://dx.doi.org/10.5741/GEMS.55.4.490

687 Vigier, M. and Fritsch, E.: More on orange luminescence in corundum, Gems Gemol., 58, 376–377,

688 2022.

689 Vigier, M., Fritsch, E., and Segura, O.: Orange luminescence of corundum as a source of geologic

690 information?, Goldschmidt 2021 Abstract, Virtual conference, 4–9 July 2021,

691 https://doi.org/10.7185/gold2021.3467, 2021a.

692 Vigier, M., Fritsch, E., and Segura, O.: Orange luminescence of corundum an atypical origin for

693 gemmologists (part one), Revue de L'Association Française de Gemmologie N° 211-Mars 2021,

694 12-19, 2021b.

695 Vigier, M., Fritsch, E., and Segura, O.: Orange luminescence of corundum an atypical origin for

696 gemmologists (part two), Revue de L'Association Française de Gemmologie N° 212-Juin 2021,

697 13-19, 2021c.

698 Vigier, M., Fritsch, E., Cavignac, T., Latouche, C., and Jobic, S.: Shortwave UV blue luminescence of

699 some minerals and gems due to titanate groups, Minerals, 13, 104,

700 https://doi.org/10.3390/min13010104, 2023.

701 Webster, R. (6th edn.): Practical gemmology. A study of the identification of gemstones, pearls, and

702 ornamental minerals, N.A.G. Press, Suffolk, USA, 92 pp., 1984.

703 Wong, W. C., McClure, D. S., Basun, S. A., and Kokta, M. R.: Charge-exchange processes in titanium-

704 doped sapphire crystals. I. Charge-exchange energies and titanium-bound excitons, Phys. Rev. B

705 Condens. Matter, 51, 5682–5692, https://doi.org/10.1103/physrevb.51.5682, 1995a.

706 Wong, W. C., McClure, D. S., Basun, S. A., and Kokta, M. R.: Charge-exchange processes in titanium-

707 doped sapphire crystals. II. Charge-transfer transition states, carrier trapping, and detrapping,

708 Phys. Rev. B Condens. Matter, 51, 5693–5698, https://doi.org/10.1103/physrevb.51.5693, 1995b.

709 Zeug, M., Nasdala, L., Wanthanachaisaeng, B., Balmer, W.A., Corfu, F., and Wildner, M.: Blue zircon
710   from Ratanakiri, Cambodia, J. Gemmol., 36, 112–132,
711   http://dx.doi.org/10.15506/JoG.2018.36.2.112, 2018.
712 Zeug, M., Nasdala, L., Chanmuang N., C., and Hauzenberger, C.: Gem topaz from the Schneckenstein
713   crag, Saxony, Germany: Mineralogical characterization and luminescence, Gems Gemol., 58, 2–
714   17, https://doi.org/10.5741/GEMS.58.1.2, 2022.